A REVIEW OF SINGLE-STATION TIME-DOMAIN POLARISATION ANALYSIS TECHNIQUES

STEVE HEARN[1,2] and NATASHA HENDRICK[1]

[1] *Exploration Geophysics Laboratory, Department of Earth Sciences, University of Queensland, Brisbane, Queensland 4072, Australia.*
[2] *Veritas DGC (Australia) Pty. Ltd., 14 Finchley Street, Milton, Queensland 4064, Australia.*

(Received December 14, 1998; revised version accepted March 2, 1998)

ABSTRACT

Hearn, S. and Hendrick, N., 1999. A review of single-station time-domain polarisation analysis techniques. *Journal of Seismic Exploration*, 8: 181-202.

Polarisation analysis is arguably the fundamental vector-processing technique applicable to multi-component reflection data. The single-station, time-domain approach is central to polarisation analysis and provides the conceptual basis for multi-station and alternative-domain extensions. This paper rationalises a number of apparently distinct single-station, time-domain algorithms that have appeared in the literature. A connection between the methods becomes apparent when each algorithm is approached in terms of optimising a vector test function. For relatively simple test functions, optimisation leads to an eigenvalue solution of normal equations. More complicated test functions are optimised using iterative search procedures. A VSP test dataset provides a comparative illustration of the performance of the various polarisation analysis algorithms examined. Polarisation parameters computed by the majority of the algorithms are strikingly similar, despite significant differences in computation approaches. The eigenanalysis method is favoured for standard polarisation analysis of high-volume datasets envisaged in future multi-component seismic reflection.

KEY WORDS: polarisation analysis, multi-component seismology, VSP.

INTRODUCTION

Multi-component seismic recording has been available to the hydrocarbon exploration industry for several decades. Processing schemes, however, have often simply involved application of single-component scalar techniques to each component individually. There is considerable scope for exploitation of the true vector nature of these data.

0963-0651/99/$5.00

Triaxial recordings contain a wealth of information on the particle motion of seismic wave modes, which can ultimately lead to improved understanding of structural and geological properties of the host rock. The fundamental vector processing technique is *polarisation analysis*, the method by which wavefield particle motion is quantitatively described.

Polarisation analysis of the vector wavefield yields at least three parameters that define particle motion. *Linearity* quantifies the degree of linear alignment of the particle motion, and hence can be used to discriminate between those waves exhibiting strongly linear particle motion (e.g., isolated compressional (P), shear (S) or Love waves), and interfering wave types or waves with elliptical particle motion (e.g., Rayleigh waves). *Azimuth* and *dip* together describe the direction of particle motion, and can be used in determining the wave type (e.g., P or S), approach direction of the wave, or orientation of geological features influencing particle-motion polarisation.

Polarisation analysis has been applied to locate earthquake epicentres (Archambeau and Flinn, 1965; Archambeau et al., 1966; Magotra et al., 1987; Ruud et al., 1988), selectively reject unwanted noise events such as ground roll and out-of-plane energy (Perelberg and Hornbostel, 1994), extract pure P- and S-wave sections (Perelberg and Hornbostel, 1994; Mu, 1996), and help characterise reservoirs through S-wave splitting analysis (Crampin, 1985; Macbeth and Crampin, 1991; Turner and Hearn, 1995; Suthers and Hearn, 1997).

Many of the algorithms for polarisation analysis originate from earthquake seismology (Shimshoni and Smith, 1964; Flinn, 1965; Archambeau and Flinn, 1965; Montalbetti and Kanasewich, 1970; Samson, 1977; Vidale, 1986; Magotra et al., 1987), and are primarily applicable to single-station three-component recordings. The single-station approach has also been productively demonstrated in exploration and reservoir development environments (Benhama et al., 1988; Shih et al., 1989; Shieh and Herrmann, 1990; Li and Crampin, 1991; Turner and Hearn, 1995, Suthers and Hearn, 1997). More recently, polarisation algorithms have been extended to exploit multi-station geometries (Jurkevics, 1988; Greenhalgh et al., 1990; Cho, 1991; Rutty and Greenhalgh, 1992), although the full potential of these extensions has yet to be demonstrated on real data.

The single-station time-domain approach is central to polarisation analysis, and arguably provides the conceptual basis for extensions that employ multiple stations and/or alternative domains (e.g., frequency, radon). Consequently it has received extensive coverage in the geophysical literature. One aim of this paper is to rationalise a number of the more widely used, and apparently distinct, algorithms. We do this by examining polarisation analysis algorithms in the geometric context of optimum positioning of a test vector. This approach

enables clarification of the relationships that exist between the different algorithms. In addition, we compare polarisation parameters obtained when the different algorithms are applied to a real VSP data example.

REVIEW OF METHODS

Overview

In the review to follow we attempt to rationalise a number of the single-station time-domain polarisation analysis algorithms which have appeared in the literature. These techniques are categorised in Fig. 1. In general, these methods estimate 'average' particle motion over a specified analysis window. The unifying approach taken is to consider each of the window methods shown in Fig. 1 in terms of the optimum positioning of a test vector. Where the test function is relatively simple, a standard constrained optimisation approach leads to an eigenvalue solution of normal equations. Where the test function is more complicated, the resultant simultaneous equations are non-linear, and an iterative optimisation approach is required.

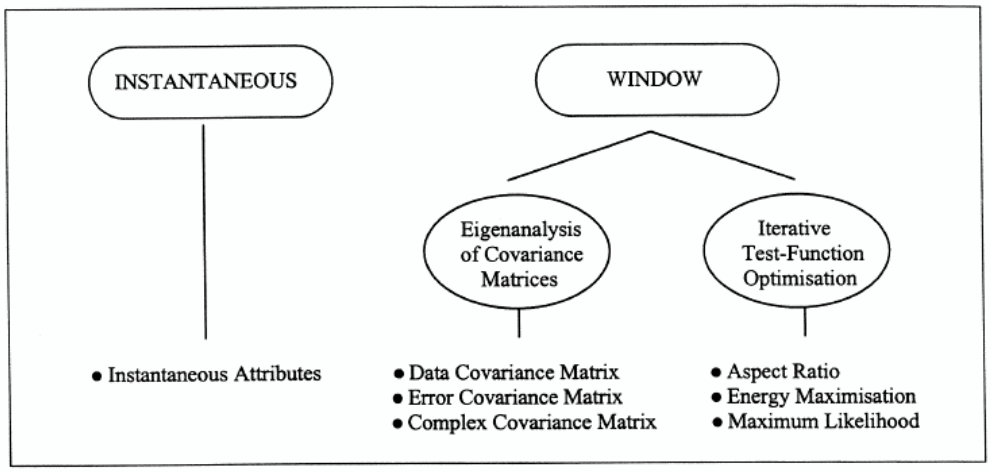

Fig. 1. Categorisation of single-station, time-domain polarisation analysis techniques.

Instantaneous Method

Instantaneous Attributes

The Instantaneous Attributes approach can be thought of as a trivial case where the analysis window is reduced to one sample. The formulation of Li and Crampin (1991) draws an analogy to the complex seismic trace analysis introduced by Taner et al. (1979), and utilises a complex seismic trace whose i-th sample is defined by:

$$f_i = x_i + jy_i = A_i e^{j\theta_i} \quad . \tag{1}$$

Here x_i and y_i are the original horizontal components, and $j = \sqrt{-1}$. A_i is termed instantaneous amplitude, while θ_i is termed instantaneous polarisation and describes particle-motion azimuth. This two-component formulation of Li and Crampin (1991) can be extended to the vertical plane to allow calculation of an instantaneous dip:

$$\phi_i = \tan^{-1}(z_i/A_i) \quad . \tag{2}$$

Here z_i is the vertical component of the seismic data.

Note that this complex-trace formulation of Li and Crampin (1991) is purely for mathematical convenience. A_i, θ_i and ϕ_i are simply the 3-D polar coordinates of the data point (x_i, y_i, z_i). Obviously, the concept of linearity does not apply in this case of unit window length.

Window Methods: Eigenanalysis of Covariance Matrices

Data Covariance Matrix (Dot Product Maximisation)

Flinn (1965) first proposed this standard eigenanalysis approach and variants have subsequently been used by Montalbetti and Kanasewich (1970), Jurkevics (1988) and Jackson et al. (1991). Commonly this approach has been presented in terms of multi-variate statistics, whereby the dependencies between data coordinates (x_i, y_i, z_i) are analysed through examination of the covariance matrix

$$\mathbf{M} = \sum_{i=1}^{N} \begin{bmatrix} x_i^2 & x_i y_i & x_i z_i \\ y_i x_i & y_i^2 & y_i z_i \\ z_i x_i & z_i y_i & z_i^2 \end{bmatrix} \quad , \tag{3}$$

where the summation is over the N samples in the data analysis window. The technique of Principle Component Analysis allows this matrix to be decomposed into a sum of three terms, constructed from three orthogonal eigenvectors ($\mathbf{u}_1$, $\mathbf{u}_2$, $\mathbf{u}_3$), namely:

$$\mathbf{M} = \lambda_1\mathbf{u}_1\mathbf{u}_1^T + \lambda_2\mathbf{u}_2\mathbf{u}_2^T + \lambda_3\mathbf{u}_3\mathbf{u}_3^T \quad , \tag{4}$$

where ^{T} denotes the vector transpose. These eigenvectors and their corresponding eigenvalues (λ_1, λ_2, λ_3) essentially define the axes of the particle-motion ellipsoid, and can be obtained as the three solutions to the characteristic equation:

$$\mathbf{Mu} = \lambda\mathbf{u} \quad . \tag{5}$$

The contribution of each term in Equation (4) is indicated by the magnitude of the associated eigenvalue. For the purposes of this paper let us define $\lambda_1 > \lambda_2 > \lambda_3$. Then for highly linear particle motion the observed covariance matrix is dominated by the large eigenvalue (λ_1), and the corresponding eigenvector [$\mathbf{u}_1 = (l_1, m_1, n_1)$] represents the prevailing particle-motion orientation. For more elliptical motion the eigenvalues are closer in magnitude.

A quantitative estimate of particle-motion linearity (L) within the analysis window is:

$$L = 1 - (\lambda_2/\lambda_1)^\gamma \quad . \tag{6}$$

L will always lie between 0 and 1, where 0 represents extremely poor linearity and 1 indicates perfectly linear particle motion. The power γ controls the sensitivity of this linearity estimator as detailed in Hendrick and Hearn (1998). A value of $\gamma = 0.5$ is used in the examples to follow. The orientation of particle motion is specified by the azimuth:

$$\theta = \tan^{-1}(m_1/l_1) \quad , \tag{7}$$

and dip:

$$\sigma = \tan^{-1}[n_1/\sqrt{(l_1^2 + m_1^2)} \quad . \tag{8}$$

Note that the technique given in Montalbetti and Kanasewich (1970) modifies the above expression for the data covariance matrix (Equation (3)) by subtracting the window mean from each seismic component before computing the covariances. This approach, which we refer to as the Debiased Data Covariance Matrix method, tends to force particle motion closer to the origin. Results generated via this modified approach are discussed below.

As an alternative to the statistically based derivation above, the eigenvalue formulation can also be derived from geometric considerations. This alternative perspective is particularly valuable in terms of relating the Data Covariance Matrix method to other polarisation analysis approaches. In brief, we attempt to find a unit vector $\mathbf{u} = (l, m, n)$ which is optimally aligned with the data vectors $\mathbf{d}_i = (x_i, y_i, z_i)$ over the analysis window. Since the dot product of two vectors represents the projection of one onto the other, this optimisation can be achieved by maximising the test function:

$$F = \sum_{i=1}^{N} (\mathbf{d}_i \cdot \mathbf{u})^2 \quad . \tag{9}$$

Differentiation of this test function with respect to l, m and n, and imposition of the constraint $l^2 + m^2 + n^2 = 1$ via the method of Lagrange multipliers, leads directly to the characteristic equation given by Equation (5).

In this geometric context the three solutions to Equation (5) correspond to test vectors for which the above test function is a maximum (and corresponding eigenvalue is maximum), a minimum (and corresponding eigenvalue is minimum), and an inflection point (for which the eigenvalue is the median).

Error Covariance Matrix (Cross Product Minimisation)

An interesting approach that can be considered 'complementary' to the preceding standard covariance matrix method was conceived by Madariaga (1967), and utilised by Mu (1996) and Suthers and Hearn (1997). By analogy with the geometric interpretation of the Data Covariance Matrix method, this technique can be thought of in terms of finding a unit vector for which the perpendicular distance to the data points is minimised, in a least-squares sense, over the analysis window. This is achieved by minimising the test function:

$$F = \sum_{i=1}^{N} |\mathbf{d}_i \times \mathbf{u}|^2 \quad . \tag{10}$$

Differentiation of this test function with respect to l, m and n, and imposition of the constraint $l^2 + m^2 + n^2 = 1$ via the method of Lagrange multipliers leads directly to the characteristic equation:

$$\mathbf{M}_E \, \mathbf{u} = \lambda \, \mathbf{u} \quad , \tag{11}$$

where

$$\mathbf{M}_E = \sum_{i=1}^{N} \begin{bmatrix} y_i^2+z_i^2 & -x_iy_i & -x_iz_i \\ -y_ix_i & x_i^2+z_i^2 & -y_iz_i \\ -z_ix_i & -z_iy_i & x_i^2+y_i^2 \end{bmatrix} \quad . \tag{12}$$

We refer to this matrix as the Error Covariance Matrix. It is related to the standard Data Covariance Matrix (**M**) via:

$$\mathbf{M}_E = P\mathbf{I} - \mathbf{M} \quad , \tag{13}$$

where $P = \sum_{i=1}^{N} (x_i^2 + y_i^2 + z_i^2)$ is the total energy in the window,

and **I** is the identity matrix.

In terms of solutions to Equation (11), the largest eigenvalue (λ_1), and corresponding eigenvector [$\mathbf{u}_1 = (l_1, m_1, n_1)$] is associated with the greatest component of *error* in the observed covariances. Conversely, the smallest eigenvalue (λ_3) and the corresponding eigenvector [$\mathbf{u}_3 = (l_3, m_3, n_3)$] is associated with the principal axis of the particle-motion ellipsoid.

In this case a measure of particle-motion linearity is given by:

$$L = 1 - (\lambda_3/\lambda_2)^{\gamma} \quad . \tag{14}$$

Again we typically use a power of $\gamma = 0.5$. The azimuth and dip of particle motion are computed using equations analogous to Equations (7) and (8), except that the appropriate eigenvector coordinates are now (l_3, m_3, n_3).

Complex Covariance Matrix

The Complex Covariance Matrix approach, proposed by Vidale (1986), is an extension of the standard Data Covariance Matrix method described above. As in the standard derivation, this approach can be geometrically related to dot product maximisation. Vidale (1986) converts the three-component seismogram (x_i, y_i, z_i) to a complex signal having components:

$$\begin{aligned} X_i &= x_i + jH\{x_i\} \\ Y_i &= y_i + jH\{y_i\} \\ Z_i &= z_i + jH\{z_i\} \end{aligned} \quad , \tag{15}$$

where H{} represents the Hilbert Transform and $j \sqrt{-1}$.

The Complex Covariance Matrix is then computed via:

$$\mathbf{C} = \sum_{i=1}^{N} \begin{bmatrix} X_i X_i^* & X_i Y_i^* & X_i Z_i^* \\ Y_i X_i^* & Y_i Y_i^* & Y_i Z_i^* \\ Z_i X_i^* & Z_i Y_i^* & Z_i Z_i^* \end{bmatrix} , \tag{16}$$

where the asterisks represent complex conjugation.

Again, the largest eigenvalue, and the corresponding complex eigenvector, define the principal axis of the particle-motion ellipsoid. Thus linearity can be estimated via Equation (6). Azimuth and dip of particle motion can be determined by equations analogous to Equations (7) and (8), except that only the real part of each eigenvector component is used.

One advantage of the Complex Covariance Matrix method, as claimed by Vidale (1986), is the stabilisation of particle motion at each point along the complex seismic trace. This is achieved via the Hilbert Transform procedure, which essentially imposes a quarter-cycle smoothing on the data. The effect of this smoothing is demonstrated in the real data example given below.

Window Methods: Iterative Test-Function Optimisation

In the previous section the vector algebraic test functions are relatively simple, and standard constrained optimisation techniques lead to an eigenvalue solution of normal equations. The techniques to follow involve more complicated test functions, resulting in non-linear simultaneous equations. The test functions are more appropriately optimised using iterative search procedures.

Aspect Ratio

In the original two-component formulation of Shih et al. (1989), the Aspect Ratio method was restricted to the estimation of the dominant azimuth of particle motion, for analysis of shear-wave splitting. A scan is performed over the range of test azimuths from 0° to 180° in order to maximise the so-called aspect ratio:

$$R_k = \sum_{i=1}^{N} s_i |\cos\theta_{ik}| \Big/ \sum_{i=1}^{N} s_i |\sin\theta_{ik}| , \tag{17}$$

where

N is the number of samples in the analysis window,
$s_i = \sqrt{[(y_{i+1} - y_i)^2 + (x_{i+1} - x_i)^2]}$,
$\theta_{ik} = \alpha_k - \psi_i$,
$\psi_i = \tan^{-1}[(y_{i+1} - y_i)/(x_{i+1} - x_i)]$.

That is, s_i is the horizontal particle-motion displacement between time samples i and i+1, and θ_{ik} is the angle between the k-th test azimuth α_k, and the particle-motion direction ψ_i. The aspect ratio R_k reaches a maximum when the test azimuth best corresponds to the true orientation of particle motion, over all samples in the analysis window.

This original formulation can be conveniently generalised to handle a full three-component polarisation analysis by introducing vector notation. This also helps clarify the relationship between the Aspect Ratio method and the other techniques discussed above. Generalisation of Equation (17) leads to the vector test function:

$$F = \sum_{i=1}^{N} |\mathbf{d}_i \cdot \mathbf{u}| \; / \sum_{i=1}^{N} |\mathbf{d}_i \times \mathbf{u}| \quad . \tag{18}$$

Note that, for consistency with the methods discussed previously, the vector position of the i-th data point $\mathbf{d}_i$ has been used in Equation (18). In terms of the original Aspect Ratio definition of Shih et al. (1989), $\mathbf{s}_i$ represents the displacement vector between the points i and i+1. This distinction will be further considered in the discussion below.

The test function given in Equation (18) is more complicated than those arising in the covariance matrix methods, and does not lend itself to an eigenanalysis solution. The required maximum can be found by iterative rotation of the test vector $\mathbf{u}$ in a three-dimensional sense. Note that this approach is extremely time consuming and an approximate solution is achieved more efficiently using a two-stage search procedure. The first stage locates the optimum $\mathbf{u}$ vector in the horizontal plane (say $\mathbf{u}_H$). The second stage of the search is then restricted to the vertical plane containing $\mathbf{u}_H$. Both the single-stage and two-stage approaches have been applied to the real data example.

Once the optimum $\mathbf{u}$ vector is determined in three-dimensional space, the particle-motion azimuth and dip can be obtained via equations analogous to Equations (7) and (8). A reasonable linearity estimate is provided by:

$$L = 1 - (1/F_{max})^{\gamma} \quad , \tag{19}$$

where F_{max} is the test function maximum for the analysis window. A power $\gamma = 0.5$ provides linearity estimates comparable to other methods, as illustrated below.

Energy Maximisation

This concept originates from the mathematical procedure used to orientate the horizontal geophones of three-component vertical seismic profiles (VSP's), in cases where an orientation device is not incorporated into the recording tool. Turner and Hearn (1995) applied the same idea to analysis of S-wave polarisation azimuths. In their two-component application a scan is performed through the range of possible azimuths. The recorded horizontal data are resolved onto two axes parallel and perpendicular to each test azimuth. The azimuth of dominant particle motion is taken as that for which the ratio of parallel to perpendicular energy is maximised over the analysis window. Generalisation of this criterion to three components using the vector notation introduced above leads to the test function:

$$F = \sum_{i=1}^{N} |\mathbf{d}_i \cdot \mathbf{u}|^2 \, / \sum_{i=1}^{N} |\mathbf{d}_i \times \mathbf{u}|^2 \quad . \tag{20}$$

As for the generalised Aspect Ratio approach $\mathbf{d}_i$ is the vector position of the i-th data point, and the optimum test vector $\mathbf{u}$ is found via either a one- or two-stage iterative procedure. Azimuth and dip are interpreted from the components of the vector $\mathbf{u}$ using Equations (7) and (8). Linearity is estimated from the maximum value of the test function within each window, using Equation (19).

Maximum Likelihood

A somewhat different approach to estimating polarisation parameters is provided by the Maximum Likelihood estimator, as used by Christofferson et al. (1988) and Roberts and Christofferson (1990). In the context of determining the polarisation of an isolated seismic event, the technique attempts to find a vector $\mathbf{u}$ that is optimally aligned with data vectors $\mathbf{d}_i$ over an analysis window. In contrast to the relatively simple geometric test functions developed above, the Maximum Likelihood criterion corresponds to minimisation of the test function (Christofferson, personal communication):

$$F = \log|\mathbf{U}| + \mathrm{tr}(\mathbf{M}\mathbf{U}^{-1}) - \log|\mathbf{M}| - 3 \quad . \tag{21}$$

Note that typographic errors occur in the original papers - Equation (5) of Christofferson et al. (1988) and Equation (32) of Roberts and Christofferson (1990).

In Equation (21), 'tr' represents the trace of the matrix and $\mathbf{M}$ is the data covariance matrix defined in Equation (3). $\mathbf{U}$ is termed the Model Covariance Matrix, whose general form is given by Equation (2) of Christofferson et al.

(1988). In our implementation we have assumed uncorrelated, equal noise energy on all three components. Under these assumptions the model covariance matrix takes the form:

$$\mathbf{U} = \begin{bmatrix} l^2E_S+E_N/3 & lmE_S & lnE_S \\ lmE_S & m^2E_S+E_N/3 & mnE_S \\ lnE_S & mnE_S & n^2E_S+E_N/3 \end{bmatrix} . \quad (22)$$

Here (l, m, n) are the components of the test vector $\mathbf{u}$. E_S and E_N are the signal and noise energies, respectively, in the analysis window. We obtain these quantities by computing the total energy in the analysis window:

$$E = \sum_{i=1}^{N} (x_i^2 + y_i^2 + z_i^2) = E_S + E_N \ , \quad (23)$$

and assuming a percentage relationship between noise and signal energies. For the examples presented below, an assumed noise percentage in the range of 0.01% to 0.1% produces a robust solution.

As is the case with the Aspect Ratio and Energy Maximisation approaches, the optimisation of the Maximum Likelihood test function (Equation (21)) is most appropriately carried out using an iterative search procedure. Again, a two-stage search provides an acceptable approximation to the full three-dimensional scan.

Azimuth and dip are interpreted from the components of the optimum test vector using Equations (7) and (8). Our tests suggest that a reasonable linearity estimate is provided by:

$$L = (F'_{min}/F_{min})^{\gamma} \ , \quad (24)$$

where F_{min} is the minimised test function value for the current analysis window, and F'_{min} is the global minimum obtained over all analysis windows. For the real data example included below a sensitivity factor $\gamma = 0.5$ yields a linearity curve broadly comparable to the other methods.

COMPARATIVE EXAMPLE

Multi-Component VSP Test Dataset

The multi-component test dataset used to compare polarisation analysis techniques is the Namgib-1 VSP from the eastern Otway Basin, southeast

Australia. These data were acquired with a dynamite source, in drilled holes offset approximately 75 m from the wellhead. Fifty-three levels were acquired over the depth interval 1375 m(KB) to 290 m(KB). A total record length of 2.0 s was recorded for each VSP level, using a sample interval of 2.0 ms.

Preprocessing prior to polarisation analysis is aimed at improving the signal-to-noise ratio without distorting relative particle motion. A minimal VSP processing sequence has been used on the Namgib-1 VSP, incorporating only horizontal geophone component orientation, band-pass filtering, shot balancing and a first-break mute. A more detailed explanation of these processes is given in Turner (1994) and Turner and Hearn (1995). Fig. 2 shows the vertical, in-line and cross-line components of the preprocessed VSP data. The direct P-wave dominates the vertical record (around 0.6 s on Level 1). The weaker downgoing events on the vertical component (0.9 s and 1.2 s on Level 1) are consistent with source-related reverberations. The dominant event on the horizontal components (1.6 s on Level 1) is interpreted as a direct S-wave, possibly generated by P-SV conversion at or near the surface. The weaker band of horizontal energy (around 1.1 s on Level 1) is consistent with a P-S conversion occurring around 300 m depth (i.e., near Level 53).

Overview of Polarisation Parameters

In order to help clarify the overall relationships that exist between these three-component seismic data and their polarisation parameters, Fig. 3 shows the computed linearity, dip, azimuth reliability measure (defined below) and azimuth for the entire Namgib-1 VSP data set. These polarisation parameters have been generated using the Data Covariance Matrix method. All results presented here have been computed using an analysis window of 50 ms.

As noted above, linearity lies in the range of 0 to 1, where 1 is representative of perfectly linear particle motion. Thus coherent, high linearity events are indicative of seismic body waves. In Fig. 3(a) the direct arrival P-wave has extremely high linearity as expected. In addition, a coherent band of high linearity is associated with the interpreted direct S-wave (1.6 s on Level 1). There is also evidence of high linearity associated with the weaker P- and S-events identified on Fig. 2.

Estimates of particle-motion dip should be examined in the light of the corresponding linearity estimates. Obviously the concept of dip is most meaningful for highly linear particle motion. When linearity is low, computed dip angles have reduced physical significance. With this consideration, the dip plot of Fig. 3(b) can be meaningfully related to the associated seismic data (Fig. 2). The obvious zone of high dips (light shading) indicates dominance of P-wave energy. As expected an abrupt change to low dip follows the arrival of the

direct S-wave. In addition, the band of low dips terminating at about 1.1 s on Level 1 reinforces the interpretation of a secondary P-S conversion mentioned above.

Just as dip estimates should be considered in conjunction with linearity, computed particle-motion azimuths should be interpreted in association with both linearity and dip. Azimuth estimates will be most reliable if linearity is high, and if the horizontal components of particle motion are significant (that is, dip is low). Fig. 3(c) shows an azimuth reliability measure (ρ) computed as a function of linearity (L) and dip (ϕ), namely:

$$\rho = L\cos\phi \quad . \tag{25}$$

This approaches unity for events having linearity equal to one or dip equal to zero, and approaches zero when linearity is zero or dip is 90°. Examination of Figs. 3(c) and 3(d) demonstrates that the most reliable azimuths are associated with the various S-wave events identified above. The most coherent band is associated with the direct S-wave (1.6 s on Level 1). These azimuth estimates (Fig. 3(d)) have been used elsewhere (Turner and Hearn, 1995) to examine S-wave splitting.

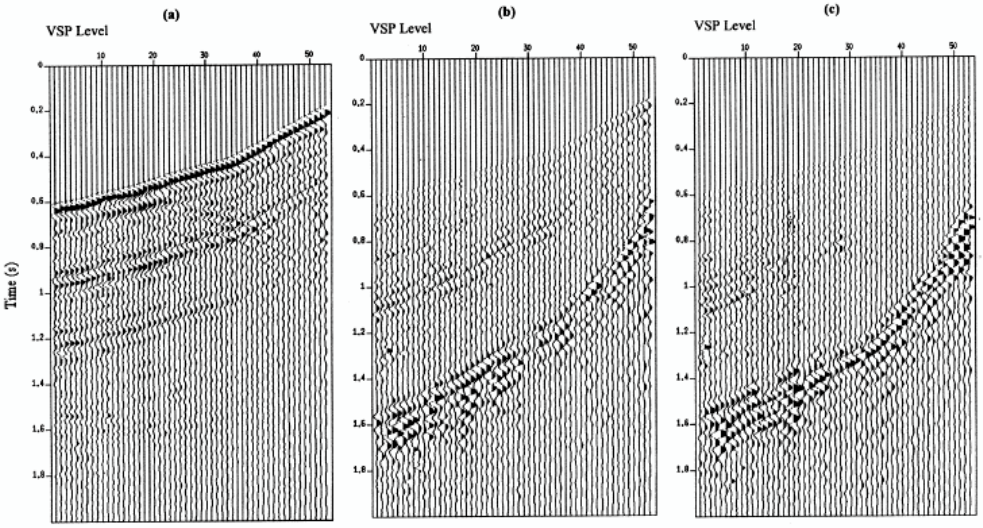

Fig. 2. Preprocessed seismic data for Namgib-1 VSP: (a) vertical, (b) in-line and (c) cross-line components. Level 1 is at 1375 m (KB) and level 53 is at 290 m (KB).

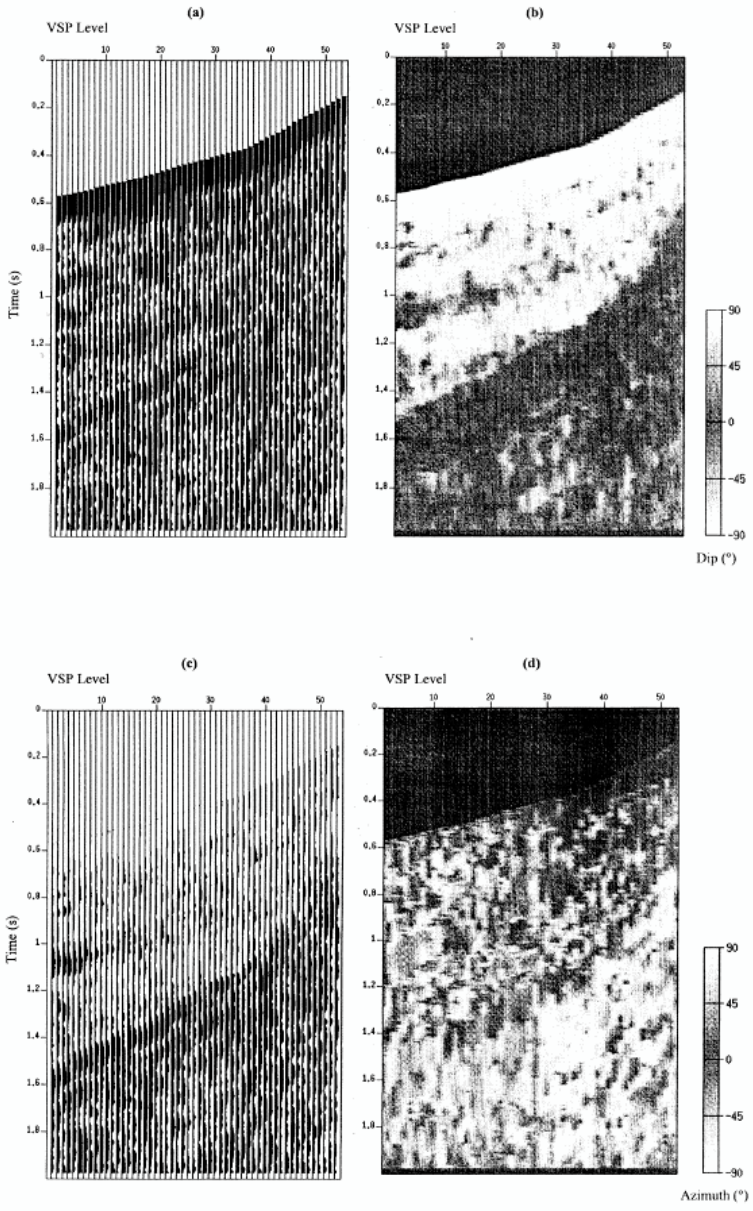

Fig. 3. Polarisation parameters for Namgib-1 VSP: (a) linearity (range of 0 to 1 on each trace); (b) particle-motion dip (°); (c) azimuth reliability measure (range of 0 to 1 on each trace) and (d) particle-motion azimuth (°). Note that here, and in subsequent figures, polarisation analysis commences at the P-wave onset, since the input data have had a first-break mute applied. The grey-scale plotting system used for dip and azimuth allows for meaningful interpretation over the range of possible angles.

Comparison of Polarisation Algorithms

Having illustrated the broad relationships that exist between the three-component data and polarisation parameters, we now compare the polarisation estimates produced by each of the algorithms discussed above. To facilitate this more detailed comparison we will concentrate on a single representative VSP level. The three-component data for Level 39 (702 m (KB)) are shown in Fig. 4. The direct P-wave is at 0.35 s, and the interpreted S-wave is at about 1.1 s. Comparison with Fig. 2 suggests that the strong energy around 0.7 s is the net effect of downgoing P-wave energy related to source reverberation, and upgoing (reflected) P-wave energy.

Fig. 5 compares the linearity estimates from the different polarisation analysis algorithms, for the section of the trace commencing at the direct P-wave onset. There is striking consistency across the methods. This lends credibility to the overall linearity interpretation, which confirms high linearity for the P- and S-wave arrivals (at 0.35 s and 1.1 s, respectively), as well as for the strong event noted at 0.7 s. Note that the Complex Covariance estimate (Fig. 5(d)) is somewhat smoother than the other estimates. As previously mentioned, this is intuitively related to the Hilbert Transform construction of the complex seismic trace. The reduced linearities at the onset of the Maximum Likelihood estimate (Fig. 5(g)) are an edge effect of the first-break mute zone.

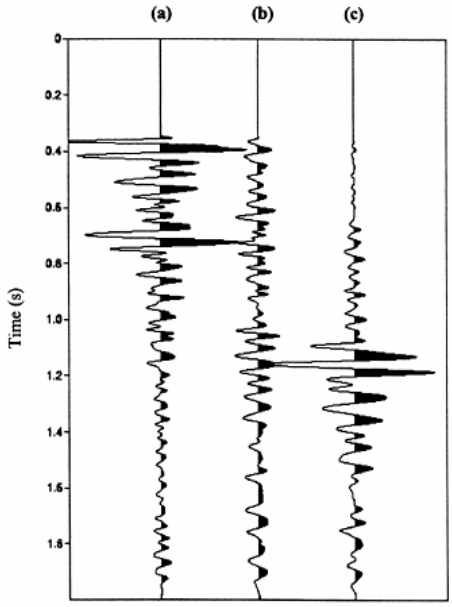

Fig. 4. Preprocessed seismic data for Level 39 (702 m (KB)), Namgib-1 VSP: (a) vertical, (b) in-line and (c) cross-line components.

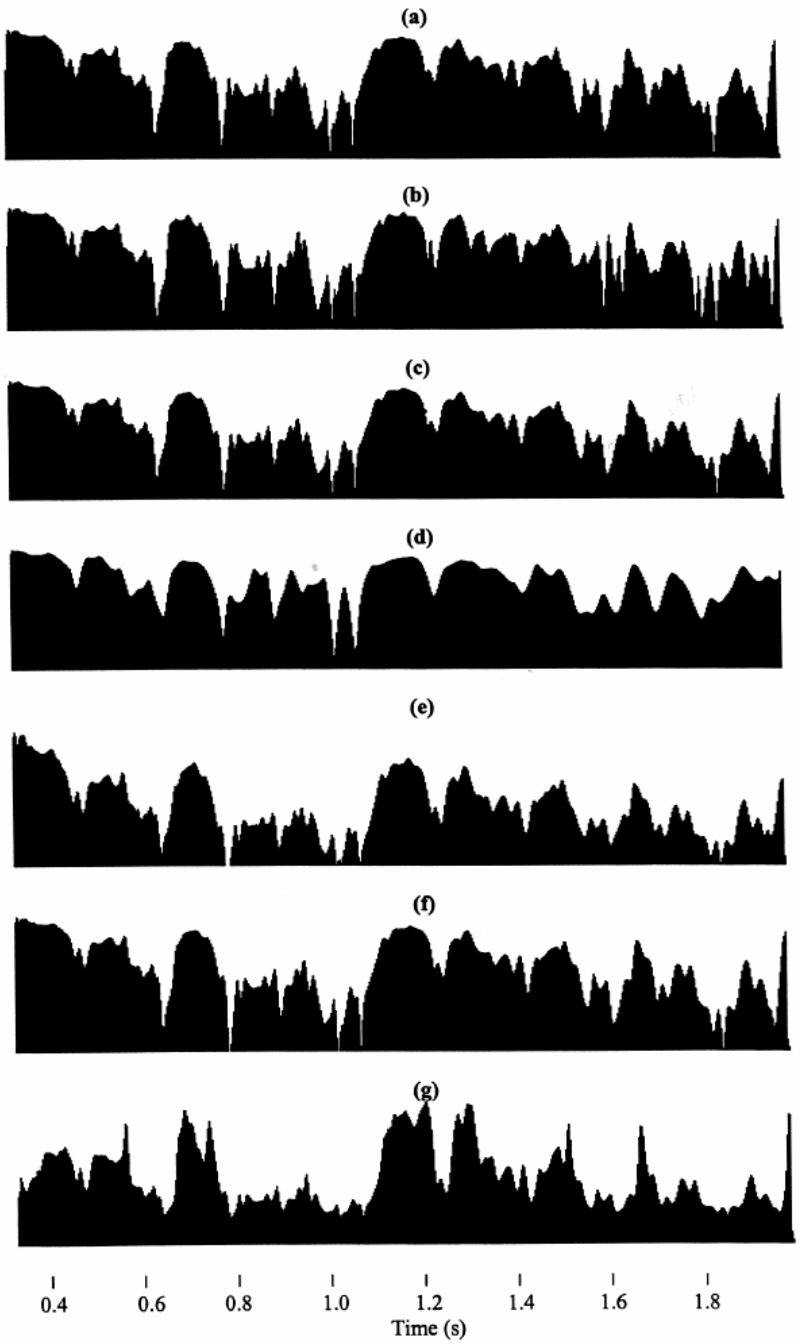

Fig. 5. Comparison of particle-motion linearity estimates for Level 39, Namgib-1 VSP computed via (a) Data Covariance Matrix, (b) Debiased Data Covariance Matrix, (c) Error Covariance Matrix, (d) Complex Covariance Matrix, (e) Aspect Ratio, (f) Energy Maximisation, and (g) Maximum Likelihood. On each plot, the vertical axis is linearity ranging from 0 to 1.

Fig. 6 compares estimates of particle-motion dip generated by the different algorithms. The reference plot of linearity (Fig. 6(a)) is included as a guide to the reliability of the dip estimates at different points along the trace. All of the window methods (Figs. 6(c)-6(i)) produce reasonably consistent dip estimates, particularly in regions of high linearity. As observed previously, these dip measurements generally indicate that the trace is dominated by near vertical P-wave energy up until the arrival of the S-wave, after which the energy is predominantly near-horizontal. As would be expected the dip angles computed via the Instantaneous Attributes approach (Fig. 6(b)) are comparatively unstable. Dip values oscillate at the dominant period of the data, effectively mirroring the alternating orientations of the particle-motion vector $\mathbf{d}_i$. Hence even for highly linear arrivals, the instantaneous dips will tend to be correct only at the extremities of particle motion (twice in any given cycle), and up to 90° in error at other points in the cycle. Again note that the Complex Covariance method shows some smoothing of results (Fig. 6(f)). Additionally, it yields one zone of conflicting dip around 0.5 s.

Estimates of particle-motion azimuth are compared in Fig. 7. The azimuth reliability measure (Fig. 7(a)) indicates that azimuth estimates are generally unreliable prior to the S-wave arrival at 1.1 s. Beyond this time all window methods (Figs. 7(c)-(i)) produce consistent, stable azimuth measurements, with the Complex Covariance method (Fig. 7(f)) again showing slightly smoothed results. Even where the reliability measure is low, a number of the methods exhibit similar azimuth measurements. This merely indicates that the different algorithms respond to noise in a similar fashion. Note that the azimuth angles computed using the Instantaneous Attributes approach (Fig. 7(b)) again oscillate at the dominant data period.

Note that in Figs. 5, 6 and 7 the Aspect Ratio, Energy Maximisation and Maximum Likelihood results have been generated using the one-stage (full three-dimensional scan) approach. Although not shown, results obtained using the two-stage approximation for these methods are very similar.

DISCUSSION

The primary aims of this paper have been to clarify the relationships that exist between a number of single-station time-domain polarisation analysis algorithms, and to compare the results of applying these various approaches to a real data example. At first glance the array of polarisation analysis techniques examined appear to have quite distinct approaches. However, the relationships between methods can be clarified if they are considered in terms of optimum positioning of a test vector with respect to the data vector, in a given analysis window. The differences between algorithms then relate directly to the different test functions used in the optimisation.

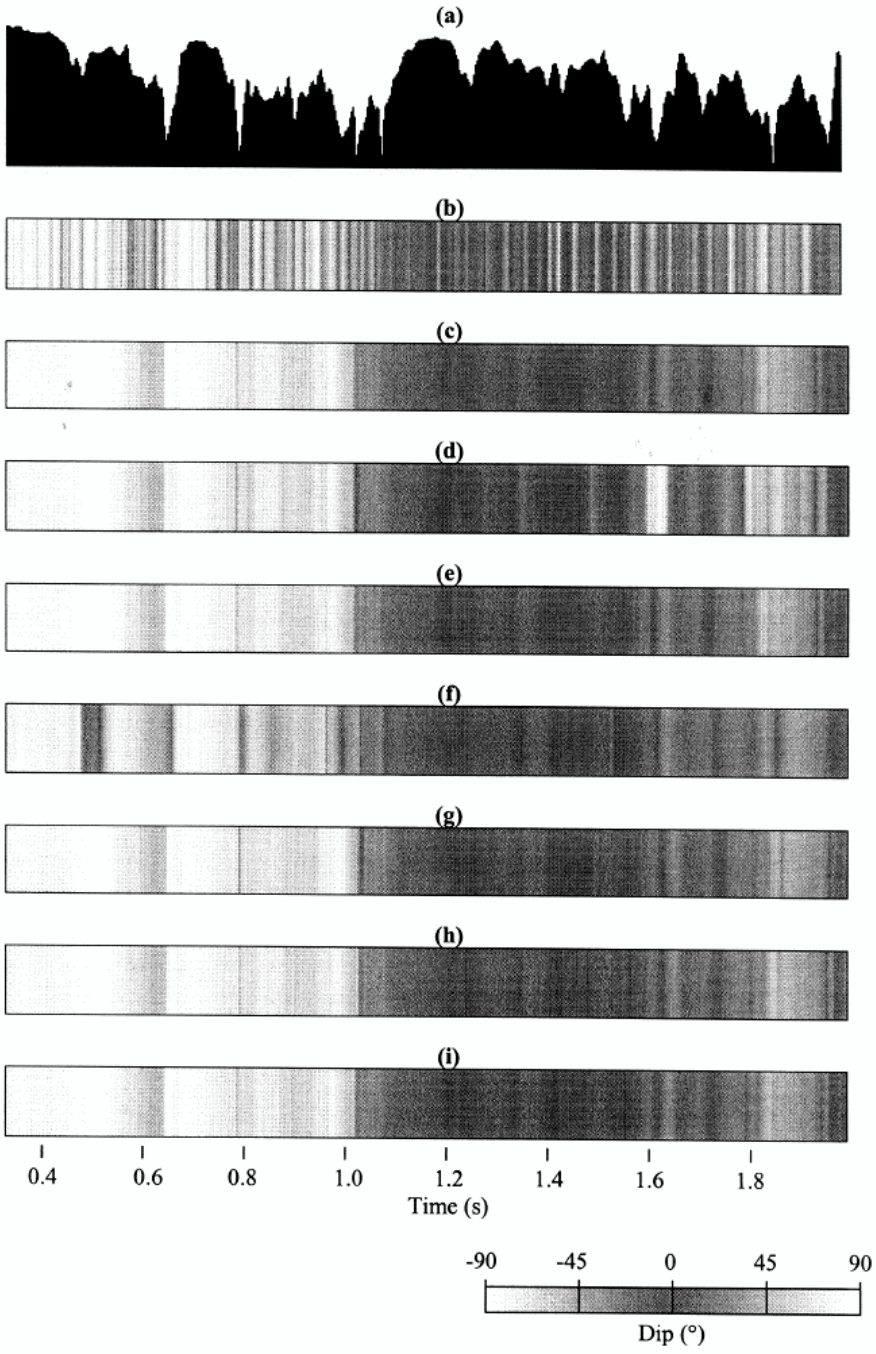

Fig. 6. Comparison of particle-motion dip estimates (°) for Level 39, Namgib-1 VSP. (a) Linearity (range of 0 to 1) indicates the reliability of dips computed via (b) Instantaneous Attributes, (c) Data Covariance Matrix, (d) Debiased Data Covariance Matrix, (e) Error Covariance Matrix, (f) Complex Covariance Matrix, (g) Aspect Ratio, (h) Energy Maximisation, and (i) Maximum Likelihood.

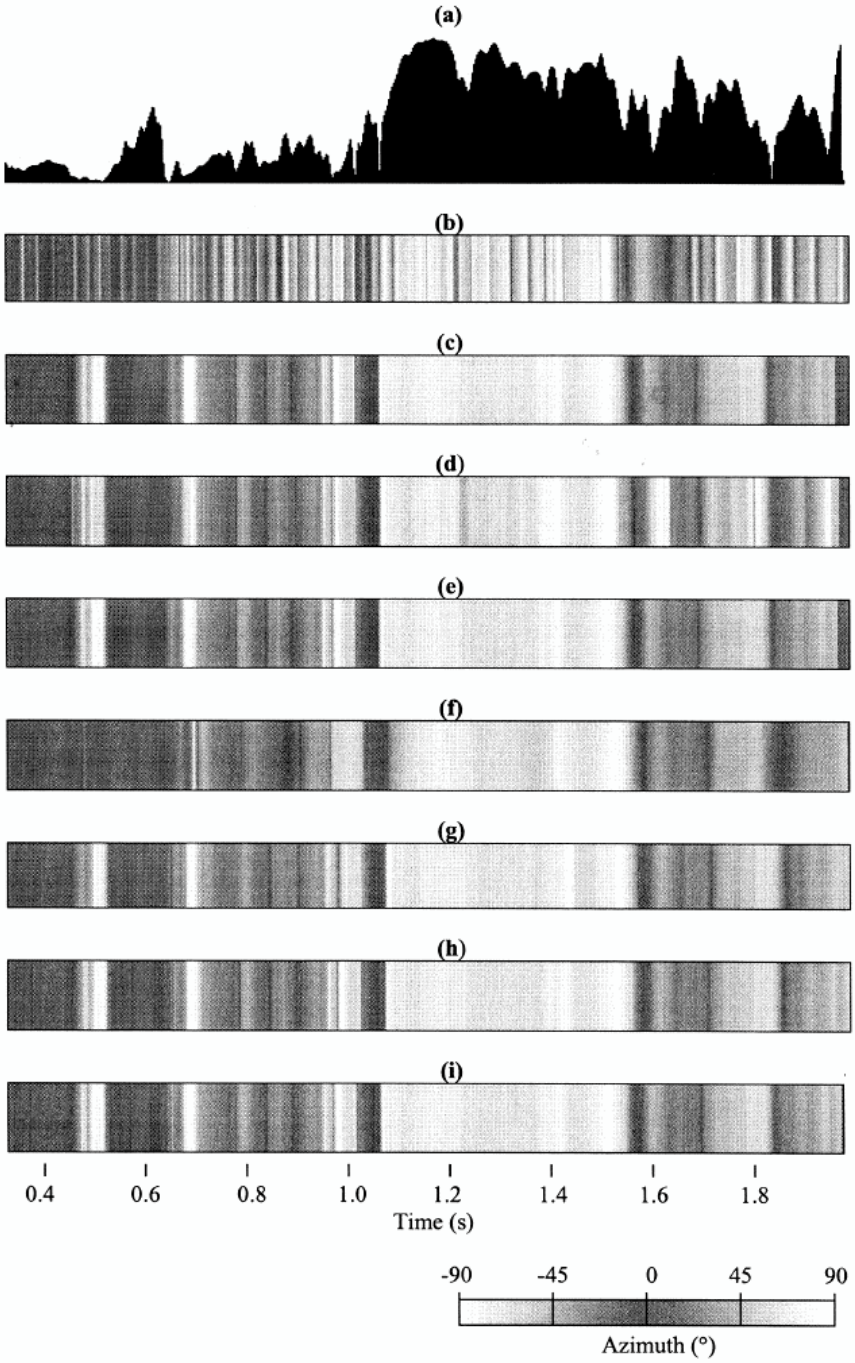

Fig. 7. Comparison of particle-motion azimuth estimates (°) for Level 39, Namgib-1 VSP. (a) Azimuth reliability measure (range of 0 to 1) indicates reliability of azimuths computed via (b) Instantaneous Attributes, (c) Data Covariance Matrix, (d) Debiased Data Covariance Matrix, (e) Error Covariance Matrix, (f) Complex Covariance Matrix, (g) Aspect Ratio, (h) Energy Maximisation, and (i) Maximum Likelihood.

As pre-empted above, a clarifying comment is warranted in relation to the usage of the data vector $\mathbf{d}_i = (x_i, y_i, z_i)$ which occurs in the various test functions. For the real data results presented above, each algorithm was implemented using $\mathbf{d}_i$, the absolute position vector of the i-th data point. As indicated in the discussion of the Aspect Ratio method, an alternative approach would be to use the vector $\mathbf{s}_i$, the displacement vector between data points i and $i+1$. For perfectly linear motion through the origin both approaches would yield the same results. However, when particle motion is not through the origin, the former approach would yield good orientation estimates at the extremities of particle motion, and less accurate estimates for data points closer to the origin. Conversely, the displacement interpretation would yield poorer estimates near the extremities of particle motion. It is interesting to note that, for the test data set used here the two interpretations yield virtually identical results. This observation is consistent with the fact that the Debiased Data Covariance Matrix method, which essentially attempts to force particle motion through the origin, yields very similar parameters to the other covariance matrix approaches (Figs. 5, 6 and 7).

Perhaps the most reassuring aspect of the study is that the different algorithms have produced very similar estimates of polarisation parameters when trialed on real VSP data. One exception has been the results from the Instantaneous Attributes approach, which understandably produces oscillatory estimates. The Complex Covariance method, on the other hand, appears capable of providing increased stability, and may prove particularly useful where window lengths need to be kept short.

Table 1. Relative compute-times for each of the single-station time-domain polarisation analysis techniques examined.

Polarisation Analysis Technique	Relative Compute-Times
Instantaneous Attributes	1
Data Covariance Matrix	2
Error Covariance Matrix	2
Complex Covariance Matrix	10
2-Stage Aspect Ratio	205
1-Stage Aspect Ratio	7000
2-Stage Energy Maximisation	214
1-Stage Energy Maximisation	7800
2-Stage Maximum Likelihood	340
1-Stage Maximum Likelihood	12000

Finally, we comment on computational requirements of the different approaches. Table 1 presents the relative compute-times for each of the techniques examined. For the iterative search procedures we have used a scan increment of 1°, and have included times for both the one-stage approach (full three-dimensional scan) and the two-stage approximation. As would be expected, the eigenanalysis methods run considerably faster than the iterative approaches.

It should be noted that the generalised Maximum Likelihood procedure, as implemented by Christofferson et al. (1988), provides some additional theoretical functionality over the other methods described here (e.g., the ability to handle multiple seismic events in a window and the provision of a 'probability estimate' for a particular wave type). However, for the standard polarisation analysis problem being considered, the eigenanalysis approach is highly favoured. This is particularly so where high-volume data sets are envisaged. This will be the case when polarisation techniques become integrated into standard surface reflection processing.

ACKNOWLEDGEMENTS

Natasha Hendrick's Ph.D. project at the University of Queensland is supported by an Australian Postgraduate Award [Industry] Scholarship. The industry partner is Veritas DGC (Australia) Pty. Ltd. The Namgib-1 VSP data were made available by the PEP-108 joint venturers Parker and Parsley (Australasia) Ltd. and GFE Resources Ltd.. The authors would like to acknowledge the support they have received from the Centre for Wave Phenomena, at the Colorado School of Mines, for the establishment of Seismic Unix at the University of Queensland.

REFERENCES

Archambeau, C.B. and Flinn, E.A., 1965. Automated analysis of seismic radiation for source characteristics. Proc. of the IEEE, 53: 1876-1884.

Archambeau, C.B., Flinn, E.A. and Lambert, D.G., 1966. Detection, analysis, and interpretation of teleseismic signals. J. Geophys. Res., 71: 3483-3501.

Benhama, A., Cliet, C. and Dubesset, M., 1988. Study and applications of spatial directional filtering in three-component recordings. Geophys. Prosp., 36: 591-613.

Cho, W.H., 1991. Decomposition of Vector Wavefield Data. Ph.D. Thesis, Texas A&M University, TX.

Christofferson, A., Husebye, E.S. and Ingate, S.F., 1988. Wavefield decomposition using ML-probabilities in modelling single-site 3-component records. Geophys. J., 93: 197-213.

Crampin, S., 1985. Evaluation of anisotropy by shear-wave splitting. Geophysics, 50: 142-152.

Flinn, E.A., 1965. Signal analysis using rectilinearity and direction of particle motion. Proc. of the IEEE, 53: 1874-1876.

Greenhalgh, S.A., Mason, I.M., Mosher, C.C. and Lucas, E., 1990. Seismic wavefield separation by multi-component tau-p polarisation filtering. Tectonophysics, 173: 53-61.

Hendrick, N. and Hearn, S., 1998. Polarisation Analysis: What is it? Why do you need it? How do you do it? Presented at the 13th Internat. ASEG Conf., Hobart. Submitted to Explor. Geophys.

Jackson, G.M., Mason, I.M. and Greenhalgh, S.A., 1991. Principal component transforms of triaxial recordings by singular value decomposition. Geophysics, 56: 528-533.

Jurkevics, A., 1988. Polarisation analysis of three-component array data. Bull. Seism. Soc, Am., 78: 1725-1743.

Li, X-Y. and Crampin, S., 1991. Complex component analysis of shear-wave splitting: theory. Geophys. J. Int., 107: 597-604.

Macbeth, C. and Crampin, S., 1991. Comparison of signal processing techniques for estimating the effects of anisotropy. Geophys. Prosp., 39: 357-385.

Madariaga, R.I., 1967. Digital Processing of Seismograms: Filters of Polarisation. M.Sc. Thesis, Universidad de Chile, Chile.

Magotra, N., Ahmed, N. and Chael, E., 1987. Seismic event detection and source location using single-station (3-C) data. Bull. Seism. Soc. Am., 77: 958-971.

Montalbetti, J.F. and Kanasewich, E.R., 1970. Enhancement of teleseismic body phases with a polarisation filter. Geophys. J. R. Astr. Soc., 21: 119-129.

Mu, L., 1996. Seismic Applications of Multi-Component Wavefield Separation Techniques. M.Sc. Thesis, University of Queensland, Australia.

Perelberg, A.I. and Hornbostel, S.C., 1994. Applications of seismic polarisation analysis. Geophysics, 59: 119-130.

Roberts, R.G. and Christofferson, A., 1990. Decomposition of complex single-station three-component seismograms. Geophys. J. Int., 103: 55-74.

Rutty, M.J. and Greenhalgh, S.A., 1992. Multi-component seismic event correlation in coherent noise. Exploration Geophysics, 23: 287-292.

Ruud, B.O., Husebye, E.S., Ingate, S.F. and Christofferson, A., 1988. Event location at any distance using seismic data from a single three-component station. Bull. Seism. Soc. Am., 78: 308-325.

Samson, J.C., 1977. Matrix and Stokes vector representations of detectors for polarised waveforms: theory, with some applications to teleseismic waves. Geophys. J. R. Astr. Soc., 51: 583-603.

Shieh, C-F. and Herrmann, R.B., 1990. Ground roll: rejection using polarisation filters. Geophysics, 55: 1216-1222.

Shih, X.R., Meyer, R.P. and Schneider, J.F., 1989. An automated, analytical method to determine shear-wave splitting. Tectonophysics, 165: 271-278.

Shimshoni, M. and Smith, S.W., 1964. Seismic signal enhancement with three component detectors. Geophysics, 29: 664-671.

Suthers, B. and Hearn, S., 1997. Shear-wave splitting analysis of multi-offset coal VSPs in the Bowen Basin. Exploration Geophysics, 28: 363-368.

Taner, M.T., Koehler, F. and Sheriff, R.E., 1979. Complex seismic trace analysis. Geophysics, 44: 1041-1063.

Turner, B.J.T., 1994. Fracture Determination from Shearwave Splitting Analysis of Single-Source Vertical Seismic Profiles. Hons. Thesis, University of Queensland, Australia.

Turner, B. and Hearn, S., 1995. Shear-wave splitting analysis using a single-source dynamite VSP in the Otway Basin. Exploration Geophysics, 26: 519-526.

Vidale, J.E., 1986. Complex polarisation analysis of particle motion. Bull. Seism. Soc. Am., 76: 1393-1405.